Solid-State Electronics 53 (2009) 935–939

Contents lists available at ScienceDirect

Solid-State Electronics

journal homepage: www.elsevier.com/locate/sse

Comparison of *p-i-n* and *n-i-n* carbon nanotube FETs regarding high-frequency performance

D.L. Pulfrey *, Li Chen

Department of Electrical and Computer Engineering, University of British Columbia, Vancouver, BC, Canada V6T 1Z4

ARTICLE INFO

Article history:
Received 15 August 2008
Received in revised form 12 May 2009
Accepted 17 May 2009
Available online 25 June 2009

The review of this paper was arranged by Dr. Y. Kuk

Keywords:
Carbon nanotube
Field-effect transistors
High-frequency
n-i-n
p-i-n

ABSTRACT

The high-frequency capabilities of *p-i-n* and *n-i-n* doped-contact carbon nanotube field-effect transistors (CNFETs) are compared via simulations using a self-consistent, energy-dependent effective-mass Schrödinger-Poisson solver. Band-to-band tunneling, which is a characteristic feature of *p-i-n* CNFETs, can also occur in *n-i-n* CNFETs, and it is shown here that it reduces the unity-current-gain frequency f_T in the latter devices. Generally, however, f_T is higher in *n-i-n* CNFETs. For both types of device, f_T increases with the chiral index of zig-zag tubes, but for different reasons.

1. Introduction

Aggressively scaled transistors, such as nanowire FETs [1] and *n-i-n* doped-contact CNFETs [2], suffer from a large subthreshold current at high drain–source voltages due to direct source–drain tunneling, and to band-to-band tunneling (BTBT). The latter transport mechanism causes a charge pile-up in the channel and prevents the gate from effectively moving the bands to turn off the device. In order to avoid this undesirable power consumption, the *p-i-n* CNFET has been proposed [3]. This device has excited interest in the digital community because its mode of operation, BTBT, offers the possibility of inverse subthreshold slopes below the thermionic-emission limit of 60 mV/decade. In contrast to the possible achievement of low OFF currents, attainment of high ON currents may be a challenge because of the restrictive nature of the tunneling transport mechanism. Nevertheless, high ON/OFF current ratios have been predicted, and the suitability of these devices to low-power applications has been suggested [4,5]. These attributes depend on the suppression of direct source–drain tunneling, either by keeping the channel length above about 15 nm, or by limiting the drain–source bias. The desirable properties of tunnel MOSFETs have led them to be investigated in other semiconductor-material systems [6].

Here, we explore the capability of *p-i-n* CNFETs for high-frequency performance. A comparison with *n-i-n* CNFETs, for which we include the BTBT effect, is also given. An energy-dependent effective-mass (EEM) model, rather than a constant-effective-mass (CEM) model, is applied to our Schrödinger-Poisson solver [7] to achieve more accurate simulation results for devices in which high electric fields are expected to be present. This situation is likely to arise in the drain region of the device at high drain–source bias and, if not correctly treated, could lead to an underestimate of the signal delay time in this region [8], and to a corresponding overestimate of f_T [9]. We also explore the effect of chirality, thereby extending the work on *n-i-n* CNFETs that has been presented recently [10].

2. Method

2.1. Energy-dependent effective-mass model (EEM)

Flietner's energy-dependent effective-mass formulation [11] is extended to apply to energies within the bands of a carbon nanotube, rather than merely to energies within the bandgap. We write:

$$m^*(E) = \frac{m_b}{2\Delta_b}(|E - E_0| + \Delta_b), \tag{1}$$

where E_0 is the mid-gap energy level, Δ_b is one-half of the bandgap for sub-band b, and m_b is a constant, parabolic-band, effective-mass for sub-band b.

* Corresponding author.
E-mail address: pulfrey@ece.ubc.ca (D.L. Pulfrey).

0038-1101/$ - see front matter © 2009 Elsevier Ltd. All rights reserved.
doi:10.1016/j.sse.2009.05.006

In our scattering-matrix solution to compute transmission probability [12], the boundary conditions for the derivative of the wavefunction need to include $m^*(E)$ to satisfy current conservation:

$$\frac{1}{m_i^*(E)}\frac{\partial\psi_i}{\partial x}\bigg|_{x=x_{ij}} = \frac{1}{m_j^*(E)}\frac{\partial\psi_j}{\partial x}\bigg|_{x=x_{ij}}, \tag{2}$$

where x_{ij} is the position of the interface between piece-wise rectangular layers i and j. The wavevector in the nanotube is given by:

$$k = \sqrt{2m^*(E)(|E-E_0| - \Delta_b)}/\hbar. \tag{3}$$

The charge densities can by expressed as:

$$Q(z,E) = q\sum_b D_b[\mathscr{G}_{S,b}(z,E)(u-f_S) + \mathscr{G}_{D,b}(z,E)(u-f_D)], \tag{4}$$

where D_b is the degeneracy of sub-band b, $\mathscr{G}_{C,b}$ is the local density of states arising from coupling to contact C [8], and f_C is the Fermi function at contact C. The parameter u is used to differentiate between electrons and holes:

$$u(z,E) = \begin{cases} 0, & E > E_0(\text{electron}), \\ 1, & E < E_0(\text{hole}). \end{cases}$$

2.2. Maximum band velocity v_{max} for zig-zag CNTs

In view of the importance of the band-limited velocity in determining the upper-bound to f_T in FETs [9], we examine here the maximum band velocity v_{max} in zig-zag CNTs:

$$v_{max} = \frac{1}{\hbar}\left(\frac{dE}{dk}\right)\bigg|_{max,b}. \tag{5}$$

The E–k relationship in sub-band b of a zig-zag tube of chiral index $(n,0)$ can be expressed from Tight-binding theory [13]:

$$E = \gamma\sqrt{1 + 4\cos\left(\frac{3ak}{2}\right)\cos\left(\frac{\pi p}{n}\right) + 4\cos^2\left(\frac{\pi p}{n}\right)}, \tag{6}$$

where k is the longitudinal wavevector, $a = 0.142$ nm is the carbon–carbon bond length, p is an integer from 1 to $2n$ indicating the different bands, and γ is the overlap parameter.

From Eqs. (5) and (6), v_{max} in the first sub-band, and the energy E_a at which it is achieved, can be expressed as [14]:

$$\text{For } (3i+1,0) \text{ tube}, \quad v_{max} = \frac{3a}{2\hbar}\gamma,$$

$$E_a = \gamma\sqrt{4\cos^2\left(\frac{2i+1}{3i+1}\pi\right) - 1},$$

$$\text{for } (3i+2,0) \text{ tube}, \quad v_{max} = -\frac{3a}{\hbar}\gamma\cos\left(\frac{2i+1}{3i+2}\pi\right),$$

$$E_a = \gamma\sqrt{1 - 4\cos^2\left(\frac{2i+1}{3i+2}\pi\right)},$$

where i is an integer. v_{max} in the first band for zig-zag nanotubes $(n,0)$ is drawn in Fig. 1. It can be seen that $v_{max} = 9.1 \times 10^5$ m s^{-1} for tubes of chirality $(3i+1,0)$, and that the maximum value increases towards this peak for $(3i+2,0)$ tubes. It has been shown recently that the reason why zig-zag tubes in these two categories exhibit different properties has its origin in the zone-folding scheme used to calculate the band structure of nanotubes from that of graphene [15].

3. Results and discussion

Simulation results are presented for coaxial, doped-contact CNFETs made from (22,0) nanotubes. In all cases, the gate length is 16 nm (to avoid direct source–drain tunneling [5]), the gate thickness is 1 nm, the oxide thickness is 3.2 nm, the oxide relative permittivity is 3.9, and the source and drain lengths are 50 nm. The source and drain contact doping densities are 0.5 nm^{-1} for both the n- and p-type regions of the n-i-n and p-i-n CNFETs that are to be compared. These specifications are similar to those for devices used in a study of switching performance [5], with the notable exception of the relative permittivity of the gate dielectric. We use 3.9, as opposed to the value of 16 used in [5], as this reduces the intrinsic capacitances, thereby improving f_T [9].

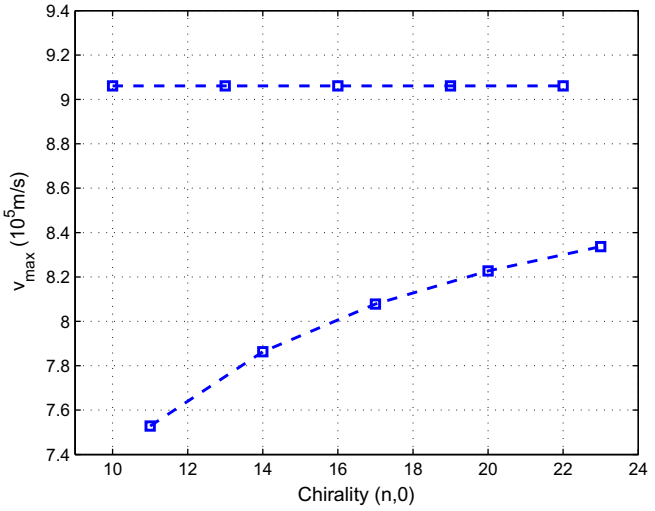

Fig. 1. Dependence of maximum, band structure limited velocity on chirality for zig-zag nanotubes, i.e. of chirality $(n,0)$. The top trace is for $n = 3i + 1$, and the bottom trace is for $n = 3i + 2$.

Fig. 2 compares the band-determined velocity dispersion relationship from the two effective-mass models with that calculated from a Tight-binding, nearest-neighbor calculation using $\gamma = 2.8$ eV. It can be seen that an energy-dependent effective-mass approach is necessary if the velocity is to be correctly modeled at energies above about 0.1 eV. As V_{DS} is increased, electrons will attain and exceed this energy on entering the drain. Thus, use of the

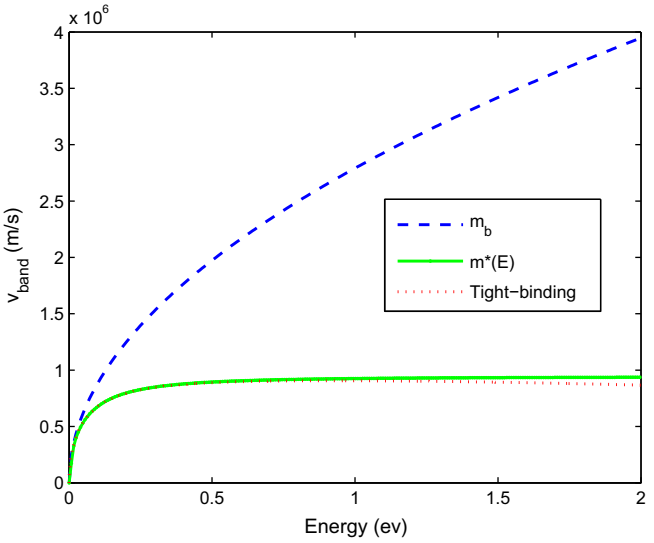

Fig. 2. Energy dependence of v_{band}, as computed from a tight-binding calculation (dotted line), and Hamiltonians using either an energy-dependent effective-mass (solid line), or a constant effective-mass (dashed line). Results are for the first sub-band of a (22,0) tube.

constant-effective-mass model will overestimate the velocity in this region, leading to an underestimate of the signal delay time in the drain [8], and, consequently, to an over-optimistic value of f_T. This fact is demonstrated in Fig. 3. The effect is more severe in the *p-i-n* case because of the opening-up of another high-energy current path at large V_{DS}, as illustrated by the lower arrow in Fig. 4a. Specifically, at high bias, tunneling of electrons into the drain at energies close to that of the conduction-band edge in the drain is facilitated. This phenomena can also be viewed as tunneling of holes into the *i*-region. The holes enter this region at high-energy, so their velocity is overestimated by the constant-effective-mass model.

BTBT can also occur at high bias in *n-i-n* structures, as illustrated in Fig. 4b. The onset of this current at $V_{DS} = 0.4$ V is responsible for the rise in current shown in Fig. 5. However, in this case, the holes injected into the *i*-region cause a charge build-up that, evidently, more severely affects f_T than does the increase in current, leading to a reduction in $f_T (= \frac{\triangle I}{2\pi \triangle Q})$. This is clear from Fig. 6, and is also shown in Fig. 3.

The ambipolar nature of conduction in *p-i-n* CNFETs is well known [4], and its effect on the gate characteristic is illustrated in Fig. 7. Contrarily, the *n-i-n* device shows the more usual positive-slope relationship. The ambipolarity necessitates the re-definition of f_T as $f_T = \frac{1}{2\pi}\left|\frac{\triangle I}{\triangle Q}\right|$ for the *p-i-n* case, with the result that f_T

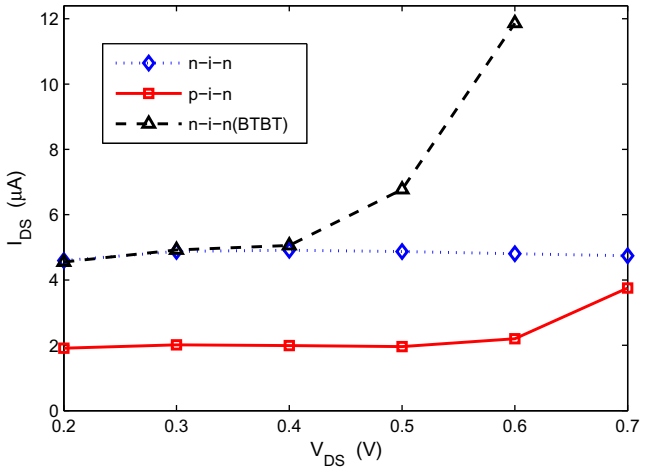

Fig. 5. Drain characteristics at $V_{GS} = 0.4$ V.

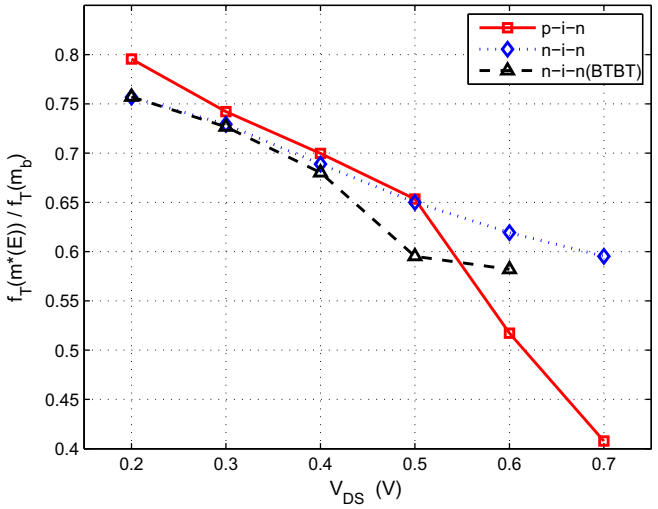

Fig. 3. Drain bias dependence of the ratio of f_T for the EEM case to that for the CEM case. The effect of including BTBT in the *n-i-n* device is also shown. $V_{GS} = 0.4$ V.

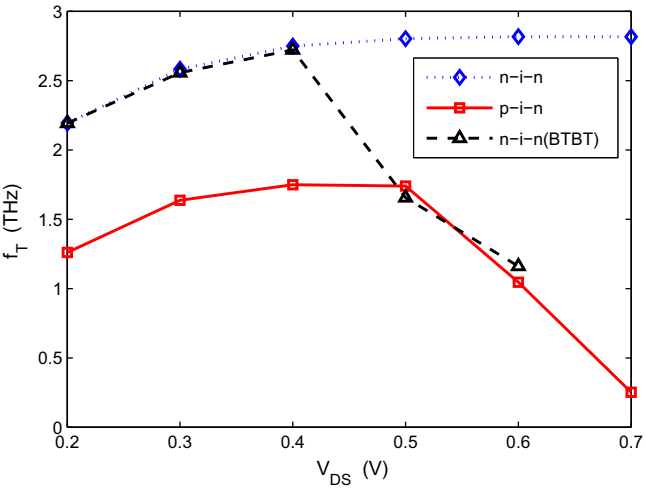

Fig. 6. Comparison of the drain bias dependence of f_T at $V_{GS} = 0.4$ V.

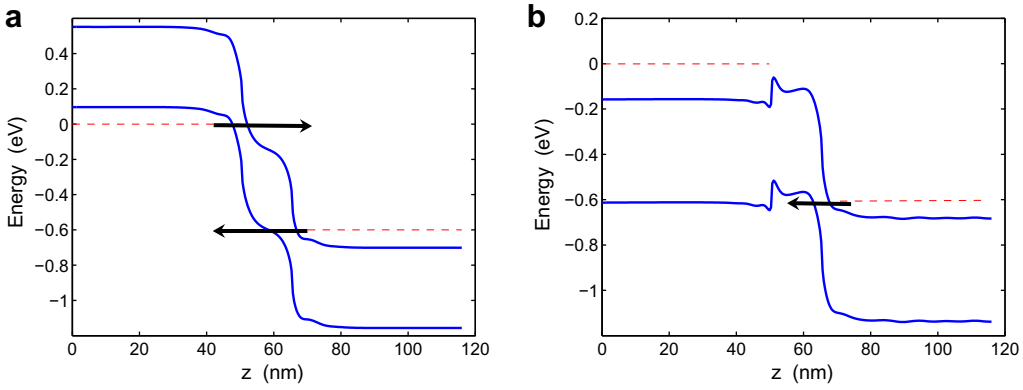

Fig. 4. Energy band diagrams at $V_{GS} = 0.4$ V and $V_{DS} = 0.6$ V for doped-contact CNFETs: *p-i-n* (left), *n-i-n* (right). In both diagrams the dashed lines are the quasi-Fermi levels in the contacts. The thick arrows denote charge flow: in (a) the top arrow is electron tunneling to the *n*-region; in both figures the left-directed flow is, effectively, holes tunneling from the *n*-region.

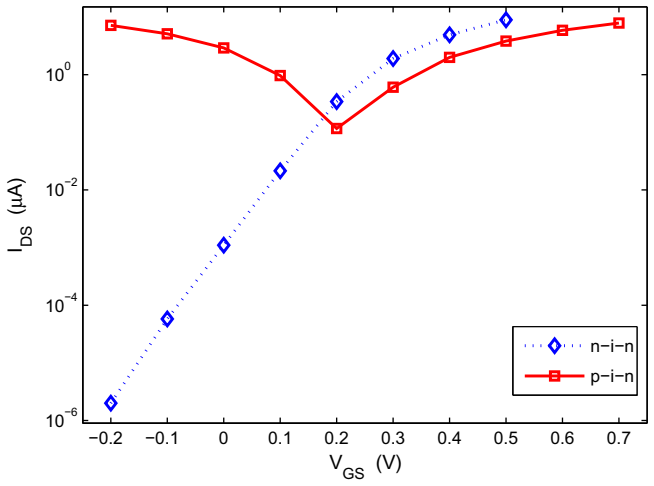

Fig. 7. Gate characteristics at $V_{DS} = 0.4$ V.

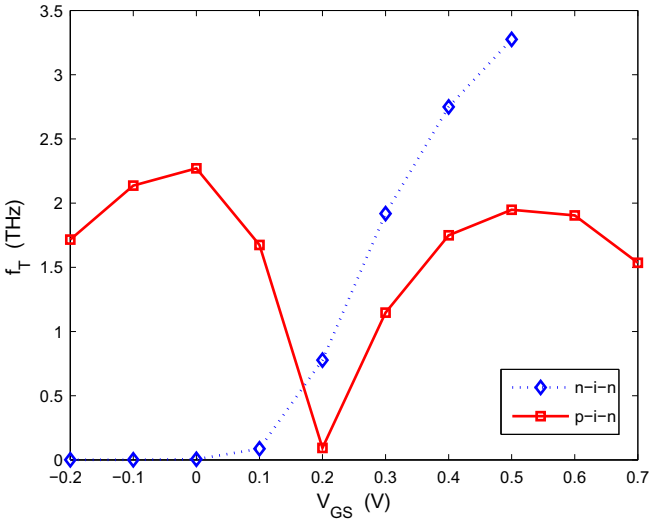

Fig. 8. Gate-bias dependence of f_T at $V_{DS} = 0.4$ V.

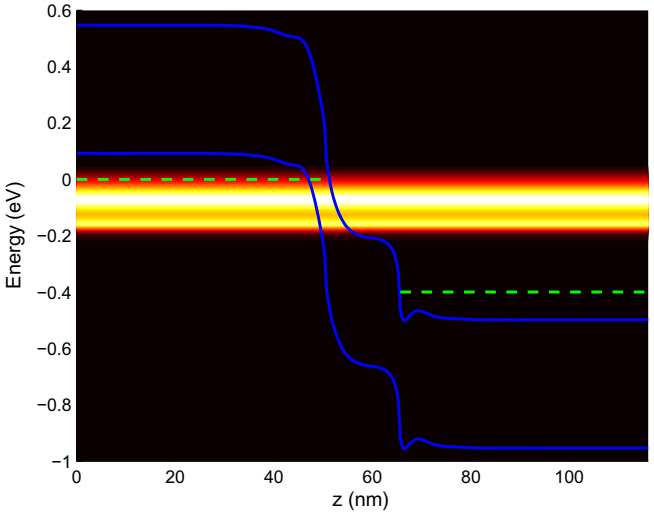

Fig. 9. Energy spectrum of the current superimposed on the energy-band diagram for the *p-i-n* CNFET at $V_{GS} = 0.5$ V, $V_{DS} = 0.4$ V. Channels of higher current are represented by lighter regions. The dashed lines are the Fermi levels in the doped-contacts, and the solid lines are the band edges.

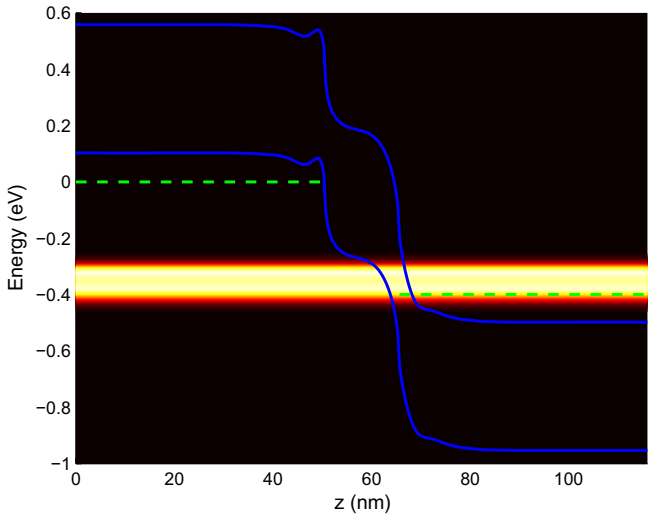

Fig. 10. Energy spectrum of the current superimposed on the energy-band diagram for the *p-i-n* CNFET at $V_{GS} = 0$ V, $V_{DS} = 0.4$ V. Channels of higher current are represented by lighter regions.

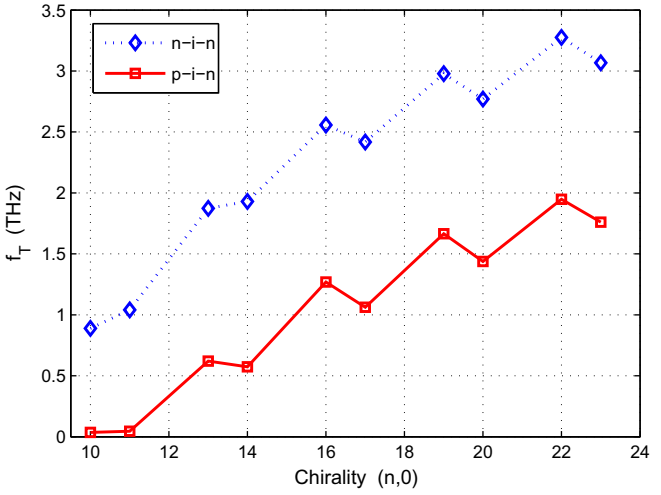

Fig. 11. f_T dependence on chirality for *n-i-n* and *p-i-n* CNFETs. $V_{GS} = 0.5$ V, $V_{DS} = 0.4$ V.

drops dramatically around the point of the current minimum (see Fig. 8), which occurs in this case at $V_{GS} = V_{DS}/2 = 0.2$ V. The different energy paths for the majority carriers (electrons at $V_{GS} > 0.2$ V, and holes at $V_{GS} < 0.2$ V), are evident in the diagrams of Figs. 9 and 10, respectively.

We now turn to the chirality-dependence of the maximum band-determined velocity v_{max}. The results are shown in Fig. 1, and the effect on f_T is shown in Fig. 11. For both the *n-i-n* and *p-i-n* devices the "oscillation" in v_{max} is manifest in f_T, but is superimposed on a steadily increasing value of f_T with chirality. In *n-i-n* devices, the increasing trend is due to a reduction of the source/intrinsic barrier height with the lower bandgap that is associated with an increase in chirality [9]. In the *p-i-n* case, the lower bandgap leads to a thinner barrier for BTBT (see Fig. 12). In each case there is an increase in transconductance with chirality. There is no associated or comparable increase in intrinsic and extrinsic capacitance, so the net effect is that f_T tracks the changes in v_{max}.

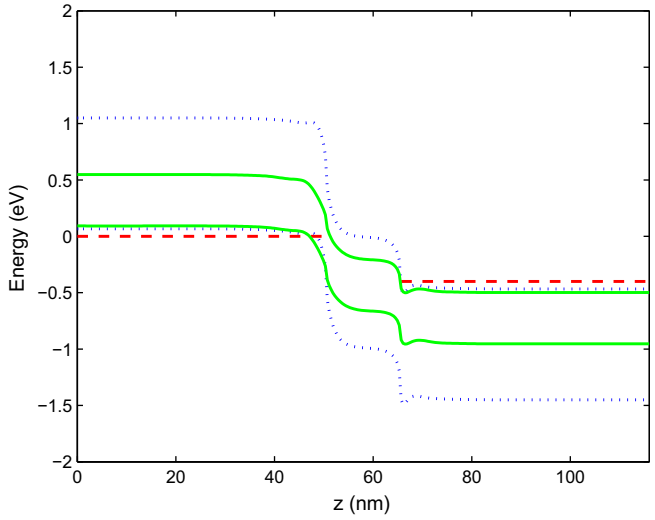

Fig. 12. Energy band diagrams at V_{GS} = 0.5 V and V_{DS} = 0.4 V for *p-i-n* CNFETs made from tubes of chirality (10,0) (dotted lines) or (22,0) (solid lines). The dashed lines are the Fermi levels in the contacts.

4. Conclusion

From this simulation study of doped-contact CNFETs it can be concluded that:

- Use of an energy-dependent effective-mass model gives less optimistic (more realistic) predictions for f_T in both *p-i-n* and *n-i-n* CNFETs than does the usual, constant-effective-mass model.
- The high-frequency performance of both *n-i-n* and *p-i-n* CNFETs employing zig-zag tubes improves with chirality.
- Operation of *n-i-n* CNFETs at high drain bias may lead to reduced high-frequency performance due to charge build-up in the device as a result of BTBT.

Acknowledgement

The financial assistance of the Natural Sciences and Engineering Research Council of Canada is gratefully acknowledged.

References

[1] Knoch J, Björk MT, Riel H, Schmid H, Riess W. One-dimensional nanoelectronic devices-towards the quantum capacitance limit. In: 66th device research conference, Santa Barbara, USA; June 2008. p. 173–6.
[2] Appenzeller J, Lin Y-M, Knoch J, Chen Z, Avouris Ph. Comparing carbon nanotube transistors – the ideal choice: a novel tunneling device design. IEEE Trans Electron Dev 2005;52(12):2568–76.
[3] Appenzeller J, Lin Y-M, Knoch J, Avouris Ph. Band-to-band tunneling in carbon nanotube field-effect transistors. Phys Rev Lett 2004;93(November):196805.
[4] Koswatta SO, Nikonov DE, Lundstrom MS. Computational study of carbon nanotube pin-tunnel FETs. IEDM Tech Dig 2005:525–8.
[5] Poli S, Reggiani S, Gnudi A, Gnani E, Baccarani G. Computational study of the ultimate scaling limits of CNT tunneling devices. IEEE Trans Electron Dev 2008;55:313–21.
[6] Boucart Kathy, Ionescu Adrian M. Threshold voltage in tunnel FETs: physical definition, extraction, scaling and impact on IC design. In: 37th European solid-state device research conference, Montreux, Switzerland; September 2006. p. 299–302.
[7] John DL, Castro LC, Pereira PJS, Pulfrey DL. A Schrdinger-Poisson solver for modeling carbon nanotube FETs. In: Technical proceedings of the NSTI nanotechnology conference and trade show, Boston, vol. 3; 2004. p. 65–8.
[8] Pulfrey DL, Castro LC, L John D, Vaidyanathan M. Regional signal-delay analysis applied to high-frequency carbon nanotube FETs. IEEE Trans Nanotechnol 2007;6:711–7.
[9] Pulfrey DL, Chen Li. Examination of the high-frequency capability of carbon nanotube FETs. Solid-State Electron 2008;52:1324–8.
[10] Chen Li, Pulfrey DL. Is there an opportunity for carbon nanotube FETs in very-high-frequency applications? In: 66th device research conference, Santa Barbara, USA; June 2008. p. 111–2.
[11] Flietner H. The E(k) relation for a two-band scheme of semiconductors and the application to the metal-semiconductor contact. Phys Stat Solidi (b) 1972;54:201–8.
[12] Ko David Yuk Kei, Inkson JC. Matrix method for tunneling in heterostructures: resonant tunneling in multilayer systems. Phys Rev B 1988;38:9945–51.
[13] Anantram MP, Léonard F. Physics of carbon nanotube electronic devices. Rep Prog Phys 2006;69:507–61.
[14] Chen Li. High-frequency limits of carbon nanotube transistors. M.A.Sc. thesis, The University of British Columbia; 2008.
[15] Abadir GB, Walus K, Pulfrey DL. Basis-set choice for DFT/NEGF simulations of carbon nanotubes. J Comput Electron; March 4, in press. p. 9. Available from: <http://www.springerlink.com/content/14792617256700h7/>.